

Ultralow Thermal Conductivity in Defect Pyrochlores: Balancing Mass Fluctuation Scattering and Rattling Modes

Natasha Ormerod,^a Anthony V. Powell,^{a*} Ricardo Grau-Crespo,^a Richard
Gover,^b Christina Cox^b

^a*Department of Chemistry, University of Reading, Whiteknights, Reading, RG6*

6DX

^b*AWE Plc, Reading RG7 4PR, Berks, England*

Supplementary Information

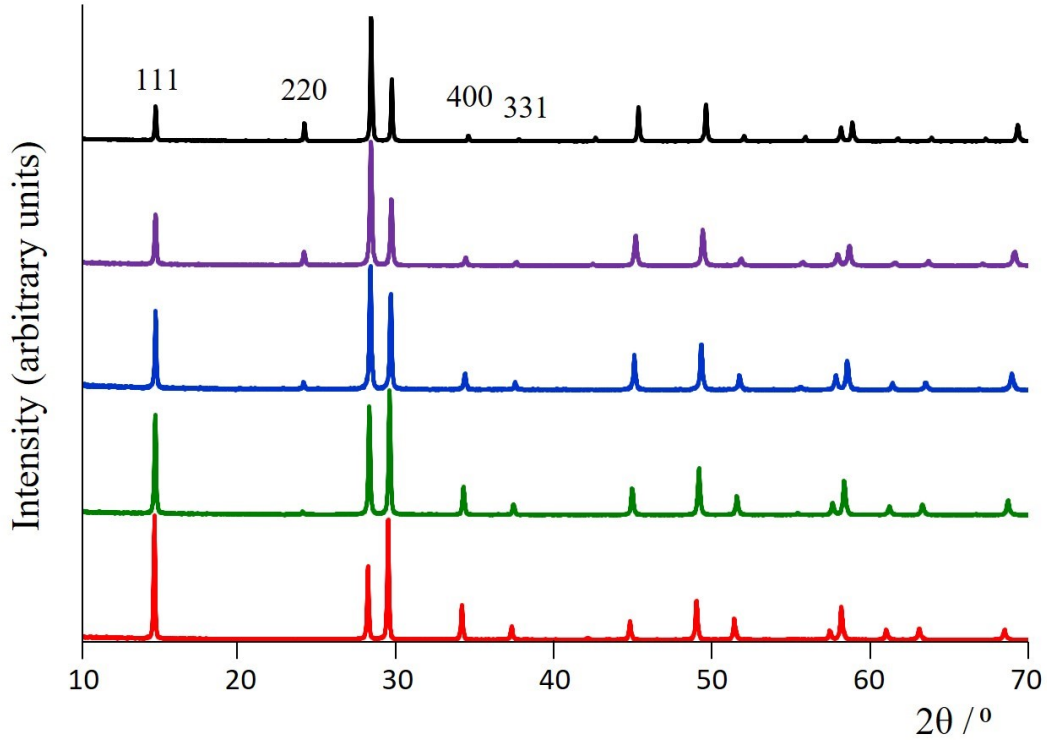


Figure S1: Laboratory powder X-ray diffraction patterns of as-prepared $K_{1-x}Cs_xTaWO_6$ ($0 \leq x \leq 1$) at 25 °C. The location of peaks $(h k l) = (111)$, (220) , (400) and (331) , the relative intensities of which change with increasing levels of caesium substitution, as noted in the text, are marked.

Table S1: Refined structural parameters of as-prepared $K_{1-x}Cs_xTaWO_6$ ($0 \leq x \leq 0.75$) determined by Rietveld analysis of synchrotron powder X-ray diffraction data collected at 25 °C.^a

x in $K_{1-x}Cs_xTaWO_6$	0.00	0.25	0.50	0.75
$a/\text{\AA}$	10.47813(2)	10.45639(1)	10.42356(1)	10.39880(5)
$K(x)$	0.4804(3)	0.4778(5)	0.4699(3)	0.4432(2)
$U_{iso}(K)/\text{\AA}^2$	0.042(2)	0.041(2)	0.044(3)	0.044(3)
$O(x)$	0.3227(3)	0.3182(2)	0.3132(1)	0.3113(3)
$U_{iso}(O)/\text{\AA}^2$	0.0261(1)	0.0240(1)	0.0293(9)	0.0293(2)
$U_{iso}(Ta/W)/\text{\AA}^2$	0.00632(1)	0.00477(9)	0.00690(5)	0.00649(7)
$R_{wp}/\%$	3.72	3.36	2.82	2.60

^a Space group: $Fd-3m$. K on $32e$ (x, x, x); Cs on $8b$ ($3/8, 3/8, 3/8$); Ta and W on $16c$ ($0, 0, 0$); O on $48f$ ($x, 1/8, 1/8$). Site occupancy factors are set at values appropriate to the nominal stoichiometry.

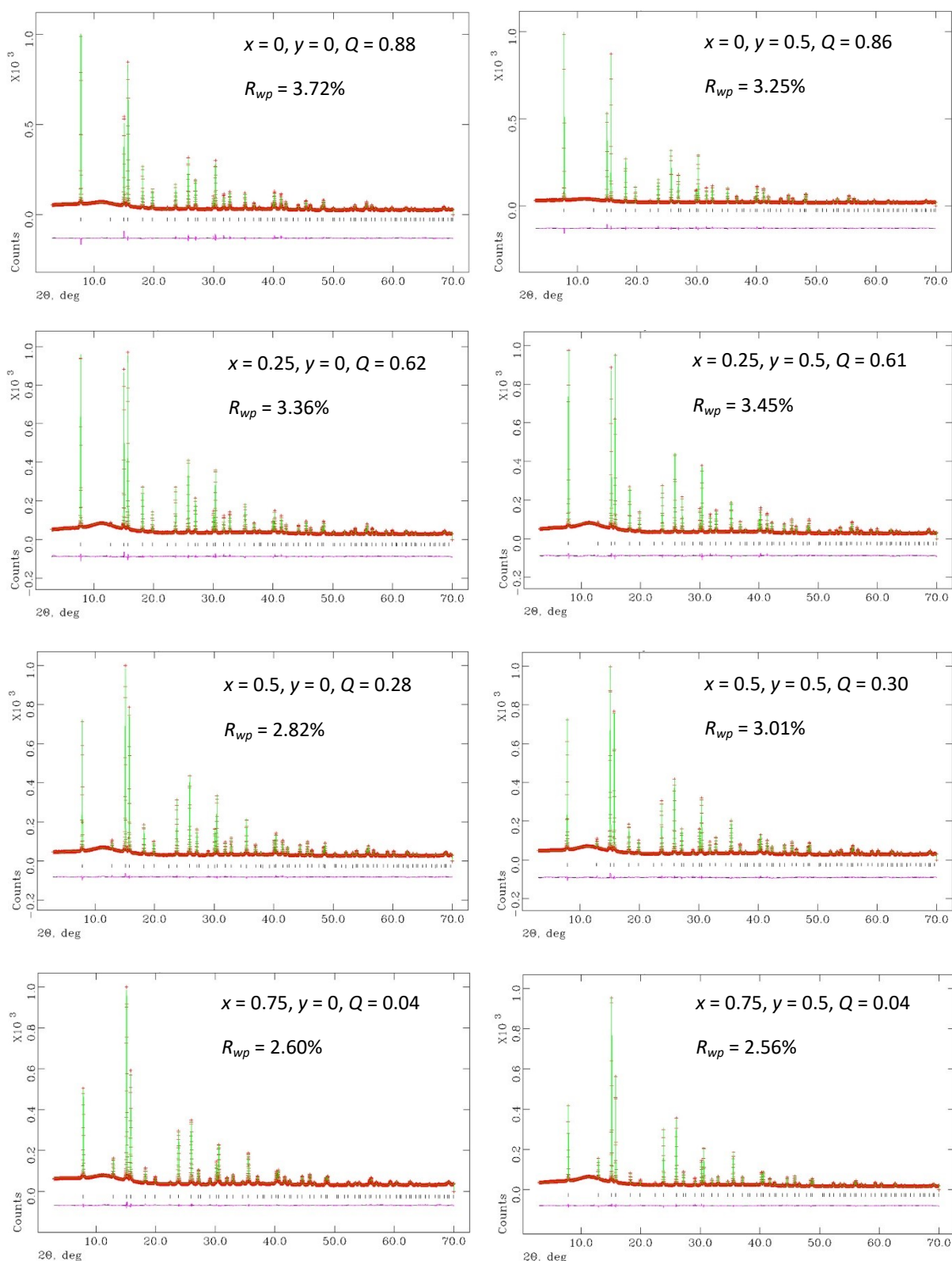


Figure S2: Final observed (red), calculated (green) and difference (pink) profiles from the Rietveld refinement of synchrotron powder X-ray diffraction data of as-prepared $K_{1-x}Cs_xTa_{1-y}Nb_yWO_6$ ($0 \leq x \leq 0.75$; $y = 0, 0.5$), collected at 25 °C. The water content (Q) per formula unit is indicated.

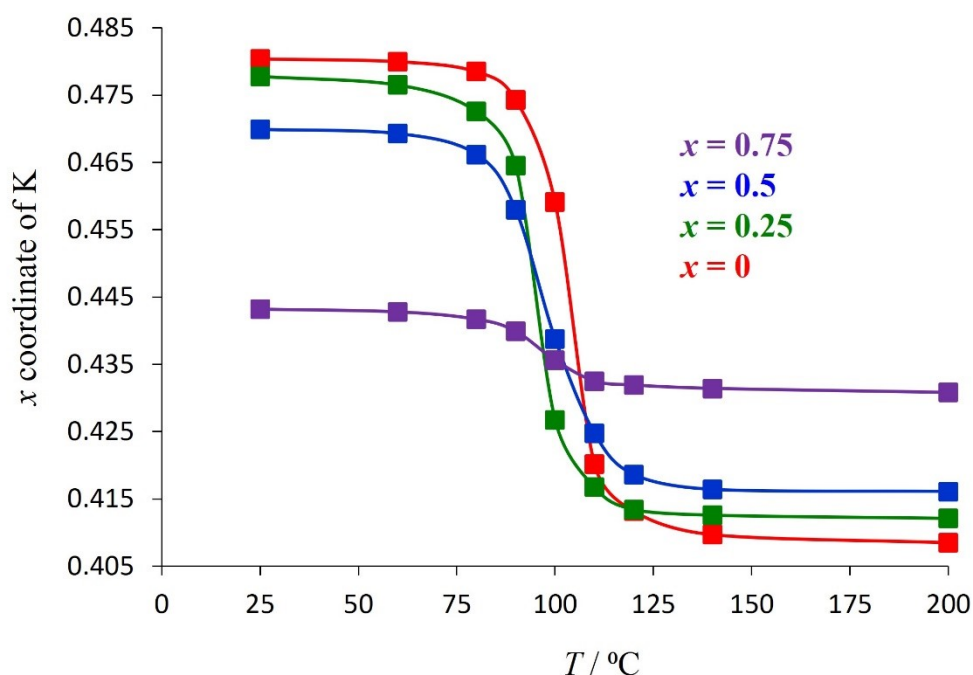


Figure S3: The temperature dependence of the potassium co-ordinate (x, x, x) in as-prepared $K_{1-x}Cs_xTaWO_6$ ($0 \leq x \leq 0.75$), determined from Rietveld analysis of synchrotron powder X-ray diffraction data collected at temperatures in the range $25 \leq T/^\circ C \leq 200$. The error bars lie within the points.

Table S2: Refined structural parameters of $K_{1-x}Cs_xTaWO_6$ ($0 \leq x \leq 0.75$) determined by Rietveld analysis of synchrotron powder X-ray diffraction data collected at $200^\circ C$.^a

x in $K_{1-x}Cs_xTaWO_6$	0.00	0.25	0.50	0.75
$a/\text{\AA}$	10.35823(3)	10.36845(2)	10.37683(7)	10.38744(1)
$K(x)$	0.4085(6)	0.4121(8)	0.4161(9)	0.4308(2)
$U_{iso}(K)/\text{\AA}^2$	0.073(4)	0.069(3)	0.0719(2)	0.070(3)
$O(x)$	0.3008(4)	0.3138(3)	0.3123(1)	0.3143(2)
$U_{iso}(O)/\text{\AA}^2$	0.0301(1)	0.0267(1)	0.0275(9)	0.0283(1)
$U_{iso}(Ta/W)/\text{\AA}^2$	0.00964(7)	0.00823(1)	0.00962(1)	0.00923(4)
$R_{wp}/\%$	2.94	2.85	2.95	2.97

^a Space group: $Fd-3m$. K on $32e$ (x, x, x); Cs on $8b$ ($3/8, 3/8, 3/8$); Ta and W on $16c$ ($0, 0, 0$); O on $48f$ ($x, 1/8, 1/8$). Site occupancy factors are set at values appropriate to the nominal stoichiometry.

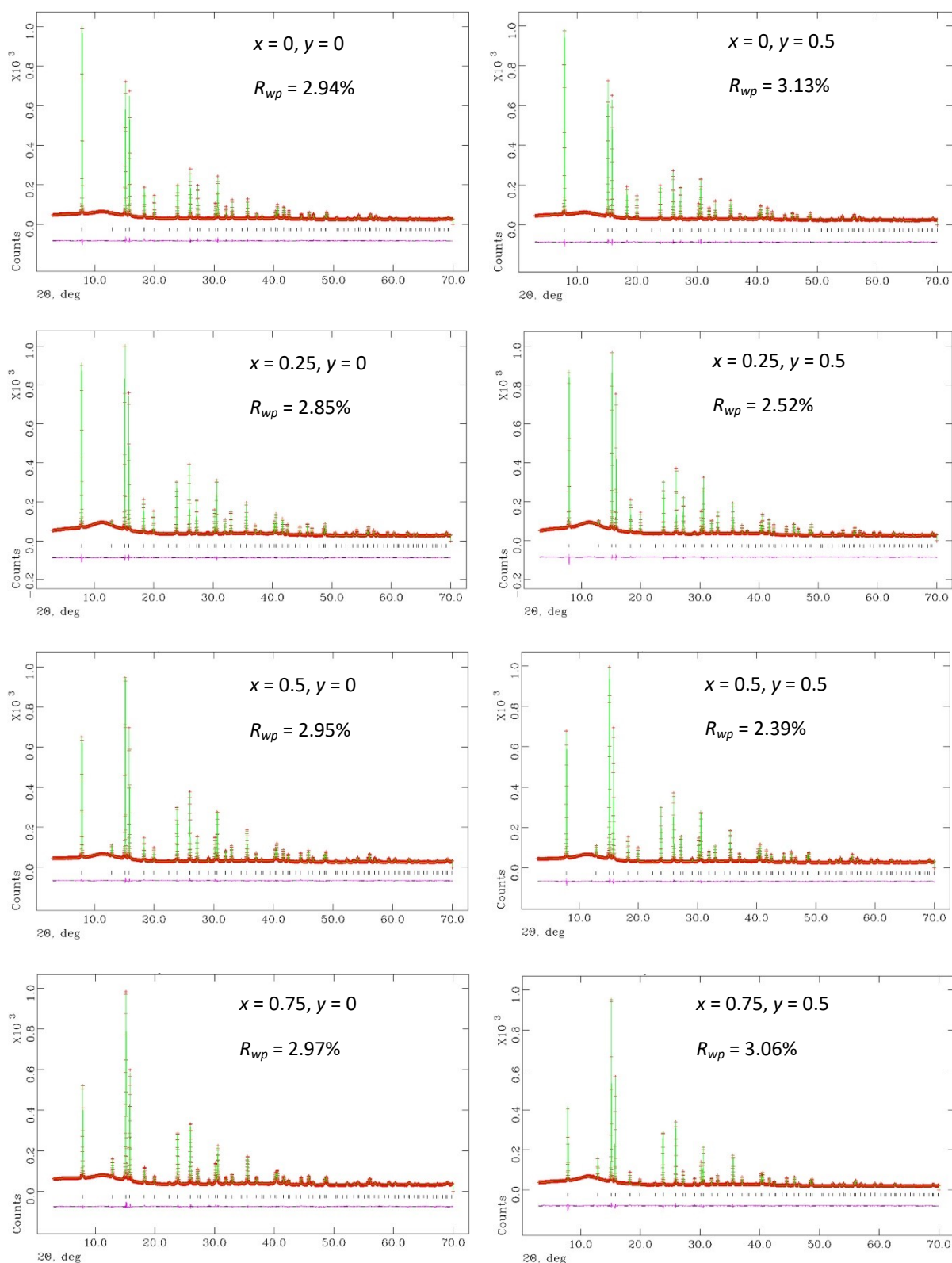


Figure S4: Final observed (red), calculated (green) and difference (pink) profiles from the Rietveld refinement of synchrotron powder X-ray diffraction data of anhydrous $K_{1-x}Cs_xTa_{1-y}Nb_yWO_6$ (0 ≤ x ≤ 0.75; y = 0, 0.5), collected at 200 °C.

Table S3: Einstein temperatures (θ_E) of the non-framework (A) cations in $K_{1-x}Cs_xTa_{1-y}Nb_yWO_6$ ($0 \leq x \leq 0.75$; $y = 0, 0.5$), determined from the temperature dependence of the atomic displacement parameter (U_{iso}) obtained from Rietveld refinement using synchrotron X-ray diffraction data collected over the temperature range $200 \leq T / ^\circ C \leq 600$.

		$\theta_E(K^+) / K$	$\theta_E(Cs^+) / K$
$x = 0$	$y = 0$	110.2	--
	$y = 0.5$	114.2	--
$x = 0.25$	$y = 0$	107.5	86.0
	$y = 0.5$	101.1	88.3
$x = 0.5$	$y = 0$	109.5	88.7
	$y = 0.5$	113.7	87.2
$x = 0.75$	$y = 0$	104.5	86.5
	$y = 0.5$	108.8	83.4

Machine-learning molecular dynamics

In order to use the Green-Kubo formula to calculate lattice thermal conductivities, we had to extend the molecular dynamics simulations to large supercells and long simulation times. For this, we fitted a machine-learned potential using the on-the-fly methodology implemented in VASP. The fitting and running required the following steps. First, we performed molecular dynamics simulations at constant pressure (0 bar) and temperature $T = 300$ K (NPT ensemble) with the Langevin thermostat, for 20,000 steps of 1 fs (total simulation time of 20 ps), during which the on-the-fly fitting of the potentials took place (this stage used a combination of ab initio and machine learning for the calculation of forces). This was followed by NPT simulations for 40 ps, with the machine learning potential only, to establish the equilibrium cell parameters at room temperature. We then performed NVT (constant volume and temperature) simulations for 40 ps, fixing the cell parameters to the values obtained in the previous step (with an augmented $8 \times 8 \times 8$ supercell). From the positions and velocities obtained, which were equilibrated at the conditions of interest, we performed a final NVE simulation (constant volume and energy), again for 40 ps, from which the heat flux was printed. These (after unit conversion) were used by the SporTran code to obtain the lattice thermal conductivities.